1. THE PHYSICS OF FORM FACTORS. THEORETICAL FRAMEWORK AND EXPERIMENTAL PROGRAMS IN A HISTORICAL PERSPECTIVE

Elastic electromagnetic processes represent an important source of information about the structure of hadrons. Their study began over forty years ago and led to a better understanding of the electrodynamics of composite particles. Deep inelastic scattering constitutes one of the experimental foundations of Quantum Chromodynamics, and, for some years, it has overshadowed the importance of form factors because of its slower decreasing cross sections. Quantum Chromodynamics is now universally believed to be the theory of strong interactions. Still, some of the most fundamental phenomena, like the binding of quarks and gluons inside hadrons or the electromagnetic properties of the proton, are not fully understood. Where the experimental feasibility has allowed to collect a large amount of data, the theory encounters technical difficulties that have been so far insurmountable. On the other hand, data is scarce (if not inexistent) where the theory is calculable. The experimental work presented in this dissertation adds a contribution to the understanding of the proton structure at the frontier of the region explored so far.

In this chapter, the physical meaning of form factors is discussed from several points of view. The peculiarities of some experimental techniques are also presented.

1.1 Introductory Remarks

Form factors are introduced to describe the structure of a composite system. They quantify the deviations from the behavior of a pointlike object, which is assumed to be known.

For example, in non-relativistic Quantum Mechanics one can study the scattering of a charged particle in the field of a static point charge. The first-order perturbative result is equal to the Rutherford cross section and depends on the kinetic energy E of the incident particle and on the scattering angle θ:

$$\left(\frac{d\sigma}{d\Omega}\right)_{\text{point}} = \frac{\alpha^2}{4E^2 \sin^4{(\theta/2)}}, \tag{1.1}$$

where α is the fine structure constant. If the pointlike charge is replaced by an extended charge distribution $\rho(\mathbf{r})$, the cross section acquires a dependence on the momentum transfer $\mathbf{q} \equiv \mathbf{k} - \mathbf{k}'$, where $\mathbf{k}$ and $\mathbf{k}'$ are the momenta of the particle before and after scattering, respectively:

$$\left(\frac{d\sigma}{d\Omega}\right)_{\text{extended}} = |F(\mathbf{q})|^2 \cdot \left(\frac{d\sigma}{d\Omega}\right)_{\text{point}}. \tag{1.2}$$

In this case, the form factor $F(\mathbf{q})$ is the Fourier transform of the charge distribution:

$$F(\mathbf{q}) = \int e^{i\mathbf{q}\cdot\mathbf{r}} \rho(\mathbf{r})\, d^3\mathbf{r}. \tag{1.3}$$

The form factor of the charge distribution being sampled can be measured by comparing the observed cross section with the calculated point cross section. In principle, one needs to measure the form factor for each value of $\mathbf{q}$

in order to extract the charge distribution. Nevertheless, if ρ is spherically symmetric and the behavior of F is known for small $\mathbf{q}$, the mean square radius can be obtained from Equation 1.3:

$$\langle r^2 \rangle = -6 \left(\frac{dF}{d\,|\mathbf{q}|^2} \right)_{|\mathbf{q}|=0} . \tag{1.4}$$

In other words, a large wavelength probe cannot resolve the detailed structure of the charge cloud, but it is sensitive to its size.

In general, the form factors are quantities used to parameterize the structure of an extended object and to interpret the experimental results. A theory that aims at explaining the structure of a composite system should in principle be able to predict its form factors. The following discussions will be focused on the electromagnetic form factors of the proton, which are the object of this dissertation.

1.2 Parameterization of the Proton Structure. Form Factors in Quantum Electrodynamics

In 1950, Rosenbluth calculated the differential cross section of elastic electron-proton scattering in the framework of recently developed QED (Rosenbluth 1950). The corresponding Feynman diagram is shown in Figure 1.1.

The incoming electron has four-momentum $k \equiv (E, \mathbf{k})$, whereas k' is its four-momentum after interacting with the proton and being deflected by an angle θ. The momentum transferred by the electron to the proton is $q \equiv k - k'$ and it is spacelike: $q^2 = -2m_p T < 0$, where T is the kinetic energy of the recoiling proton in the frame where it is initially at rest. It is often convenient to define $Q^2 \equiv -q^2$, which is positive in the spacelike region.

From now on, we will assume that the electron rest energy m_e is negligible with respect to its total energy. The momentum transfer becomes:

$$Q^2 = 2EE' \cdot \left[1 - \cos\theta - \frac{m_e^2}{EE'}\right] \tag{1.5}$$

$$\simeq 4EE' \sin^2(\theta/2) \tag{1.6}$$

$$= \frac{4E^2 \sin^2(\theta/2)}{1 + 2(E/m_p)\sin^2(\theta/2)} \tag{1.7}$$

For a given energy of the impinging electron, the maximum momentum transfer is achieved when the electron is back-scattered, but it is the energy E that sets its order of magnitude.

One of the main points in Rosenbluth's paper was to quantify the deviations from the behavior of a pointlike Dirac particle. These were taken into account by allowing the proton's charge and anomalous magnetic moment to vary as a function of the invariant momentum transfer, which is chosen as the independent kinematic quantity of the process. This is done[a]

[a] A standardized notation is used in place of the parameterization found in the original papers.

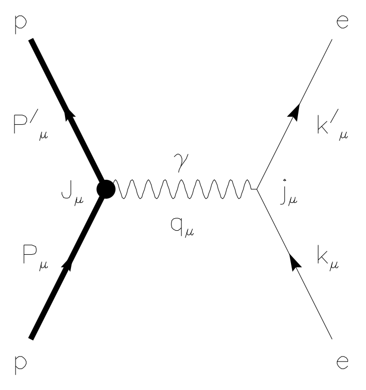

Fig. 1.1: Lowest-order Feynman diagram for elastic electron-proton scattering.

by writing the current operator J_μ in terms of the static charge e and anomalous magnetic moment κ multiplied by two functions $F_1(q^2)$ and $F_2(q^2)$:

$$J_\mu = e\left[\gamma_\mu F_1 + \frac{\kappa}{2m_p}\sigma_{\mu\nu}q^\nu F_2\right]. \tag{1.8}$$

This form is to be compared with the pointlike lepton current $j_\mu = e\gamma_\mu$. If we use the abbreviation $\tau \equiv Q^2/4m_p^2$, the resulting first-order differential cross section in the laboratory frame is known as Rosenbluth's formula:

$$\left(\frac{d\sigma}{d\Omega}\right)_R = \left(\frac{d\sigma}{d\Omega}\right)_{NS} \cdot \left[\frac{G_E^2 + \tau G_M^2}{1+\tau} + 2\tau G_M^2 \tan^2(\theta/2)\right]. \tag{1.9}$$

The subscript NS indicates the scattering of the electron off a no-structure spinless object. The corresponding cross section is the Mott cross section multiplied by a factor that takes the recoil of the proton into account:

$$\left(\frac{d\sigma}{d\Omega}\right)_{NS} = \frac{E'}{E}\cdot\left(\frac{d\sigma}{d\Omega}\right)_{Mott} = \frac{E'}{E}\cdot\frac{\alpha^2\cos^2(\theta/2)}{4E^2\sin^4(\theta/2)}. \tag{1.10}$$

In the Mott cross section, the factor $\cos^2(\theta/2)$ comes from the spin of the electron, while the rest is the familiar Rutherford expression for the scattering of a spinless particle off an electrostatic potential.

The 'electric' and 'magnetic' form factors G_E and G_M, also known as Sachs form factors, are introduced as follows:

$$\begin{aligned} G_E &\equiv F_1 + \kappa\frac{q^2}{4m_p^2}F_2 \\ G_M &\equiv F_1 + \kappa F_2. \end{aligned} \tag{1.11}$$

The physical meaning of this parameterization, already hinted at by Yennie et al. (1957), was fully investigated by Ernst, Sachs, and Wali (1960). These form factors are used because they are strictly related to the charge and magnetic moment distributions inside the nucleon. In particular, their values at $q^2 = 0$ are the static electric charge and magnetic moment of the proton:

$$\begin{aligned} e &= eG_E(0) \\ \vec{\mu} &= \frac{e}{2m_p} G_M(0)\vec{\sigma}; \end{aligned} \tag{1.12}$$

whereas their slope at the origin is proportional to the second moments of the charge and magnetic moment distributions:

$$\begin{aligned} \langle r^2_{ch} \rangle &= 6 \left. \frac{dG_E}{dq^2} \right|_{q^2=0} \\ \langle r^2_{mag} \rangle &= \frac{6}{\mu_p} \left. \frac{dG_M}{dq^2} \right|_{q^2=0} \end{aligned} \tag{1.13}$$

The expression of the current operator used by Rosenbluth (Equation 1.8) is the most general, as shown by Foldy (1952) and, under fewer restrictions, by Salzman (1955) and Yennie et al. (1957). In other words, two independent functions of q^2 are necessary and sufficient to characterize the electromagnetic properties of any spin $1/2$ particle, under the assumptions of relativistic covariance and current conservation. With time-reversal arguments, one can show that these functions can be chosen to be real for every $q^2 \leq 0$.

1.3 First Experimental Information on the Proton Structure. The Spacelike Region

Rosenbluth's work was motivated by the fact that intense electron beams were becoming available at the new Stanford linac. A wide energy range, from 6 to 1000 MeV, was accessible. The scattering from a hydrogen target could represent a test for QED and, also, a way of studying the proton structure. A systematic experimental program followed, allowing to collect a large body of data in the spacelike region (Hofstadter 1963).

McAllister and Hofstadter (1956) were the first to measure the size of the proton. The electron beam accelerated by the Stanford linac was directed towards a high-pressure hydrogen chamber, which was placed inside an evacuated vessel. The scattered electrons, after being collimated by a set of slits, entered a magnetic spectrometer, which could be moved around the target. Interpreting the number of observed counts as a function of the scattering angle according to Rosenbluth's formalism, a value of $\sqrt{\langle r^2 \rangle} = 0.74 \pm 0.24$ fm was deduced. This result relies on the assumption that the charge and magnetic moment distributions are similar.

The form factors can be separated by measuring the reduced Rosenbluth cross section, which can be defined from Equation 1.9:

$$\sigma_{\mathrm{red}} \equiv \left[\left(\frac{d\sigma}{d\Omega} \right)_R \Big/ \left(\frac{d\sigma}{d\Omega} \right)_{NS} \right] \frac{(1+\tau)\epsilon}{\tau} = \frac{\epsilon}{\tau} G_E^2 + G_M^2 \tag{1.14}$$

The quantity ϵ is a function of Q^2 and of the scattering angle and is bounded:

$$\epsilon = \left[1 + 2(1+\tau) \tan^2 (\theta/2) \right]^{-1}; \quad 0 \le \epsilon \le 1. \tag{1.15}$$

For fixed Q^2, the reduced cross section is linear in ϵ. From a fit to the data one can extract the slope G_E^2/τ and the intercept G_M^2. This procedure is known as Rosenbluth separation, and allows to measure both form factors if the momentum transfer is not too large.

The behavior of G_E and G_M has been investigated over a wide range of Q^2. Walker et al. (1994) and Andivahis et al. (1994) report recent measurements of both the electric and magnetic form factor at $Q^2 < 10$ $(\mathrm{GeV}/c)^2$ obtained at SLAC. Walker et al. (1994) have also performed a global fit to all existing data. As can be seen from Figure 1.2, the form factors can be well represented by the following empirical functional form, known as the

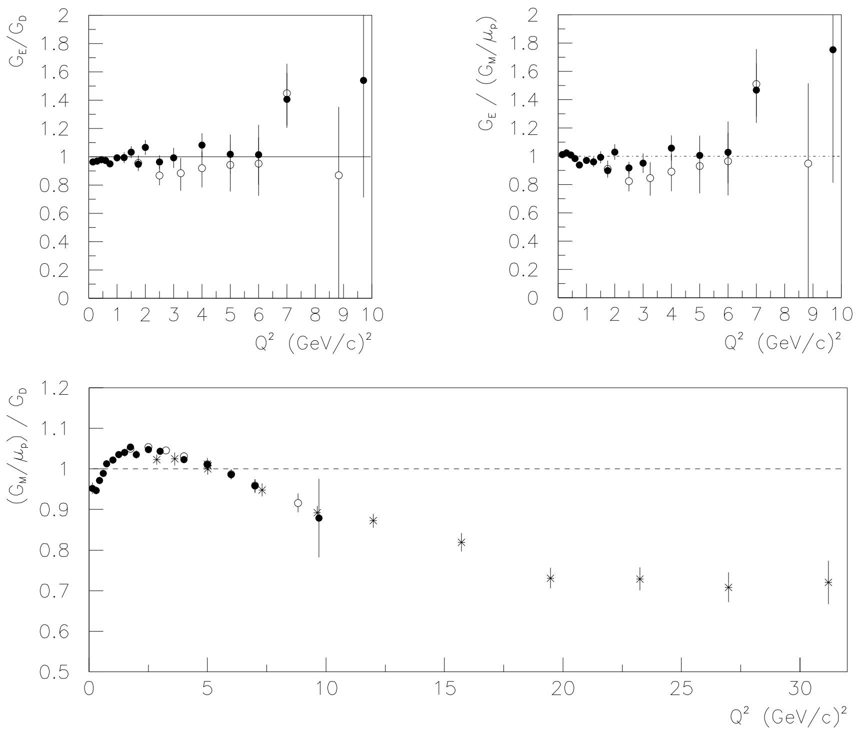

Fig. 1.2: Form factors obtained in electron-proton elastic scattering. The data at low Q^2 are from a fit to all existing measurements performed by Walker et al. (1994) (•). The mid- and high-Q^2 regions have been explored by Andivahis et al. (1994) (◦) and Sill et al. (1993) (∗), respectively.

dipole formula:

$$G_D = \left(1 + \frac{Q^2}{\Lambda}\right)^{-2} \quad \Lambda = 0.71 \text{ GeV}^2. \tag{1.16}$$

The electric and magnetic form factors are also found to scale approximately in the same way: $G_E(q^2) = G_M(q^2)/\mu_p = G_D$. Deviations from the dipole behavior and from scaling are within approximately 10% for Q^2 smaller than 10 $(\text{GeV}/c)^2$.

These facts confirmed that the electric and magnetic moment distributions are very similar. The proton root-mean-square radius (from Equation 1.13) comes out to be $\sqrt{\langle r^2 \rangle} \simeq 0.8$ fm.

At low momentum transfer, i. e. when $Q^2 \ll m_p^2$, the recoil of the proton is negligible and $E'/E \simeq 1$. In this regime, $G_E(q^2)$ can be interpreted as the Fourier transform of a charge density $\rho(\mathbf{r})$. Transforming the dipole function G_D, one gets a charge density proportional to e^{-r}.

Because of the kinematic factors in Equations 1.9 and 1.14, at high momentum transfers Rosenbluth separation cannot be performed, and only the magnetic form factor can be precisely measured. Recent data (Sill et al. 1993) taken at SLAC in this regime up to $Q^2 = 31$ $(\text{GeV}/c)^2$ indicate significant deviations from the dipole behavior, as shown in Figure 1.2.

1.4 Form Factors in the Timelike Region

At the beginning of the 1960s, the feasibility of electron-positron colliders was proven at Stanford and Frascati, opening a wide spectrum of physical investigations. A discussion of the possible experiments and of some theoretical predictions from those years, including the form factors of barions, can be found in the paper by Cabibbo and Gatto (1961).

In the same years, soon after their discovery in 1955, antiprotons became available in relatively intense beams ($\approx 10^4$ particles per pulse). A proposal was made by Zichichi et al. (1962) to study lepton-antilepton final states in antiproton-proton annihilations at CERN.

In the process

$$\bar{p}p \rightarrow e^+e^-, \tag{1.17}$$

the momentum transfer $q \equiv -(k + k')$ is directly related to the center-of-momentum (CM) energy and it is timelike: $q^2 = s > 0$. Obviously, the reaction can only take place above a certain threshold, which corresponds to $s = 4m_p^2$. By definition (Equation 1.11), at threshold G_E equals G_M.

The angular distribution of process 1.17 can be predicted using helicity arguments, introduced in an elegant article by Jacob and Wick (1959). One of their main results is an expression for the scattering amplitude $f(\theta, \phi)$ for the process $a + b \rightarrow c + d$. In general, the angular dependence can be factorized in terms of exponentials and rotation matrices $d^j(\theta)$. Each term is weighed by amplitudes expressing the dynamics of the process, which, in general, depend upon the CM energy $\sqrt{s}$, the total angular momentum J and the spin of the particles (through their helicities λ_a, λ_b, λ_c and λ_d). In symbols:

$$d\sigma = |f(\theta, \phi)|^2 \, d\Omega \tag{1.18}$$

$$f(\theta, \phi) = \frac{1}{p} \sum_J (J + 1/2) \left\langle \lambda_c \lambda_d \left| T^J(s) \right| \lambda_a \lambda_b \right\rangle e^{i(\lambda-\mu)\phi} \, d^J_{\lambda\mu}(\theta) \tag{1.19}$$

$$(\lambda = \lambda_a - \lambda_b; \ \ \mu = \lambda_c - \lambda_d), \tag{1.20}$$

where p is the relative momentum of the two particles in the initial state and T is related to the S-matrix by $S - 1 = iT$. The sum over J reflects the fact that a two-particle state $|p; \theta\phi; \lambda_1\lambda_2\rangle$ emerging at a definite angle in the CM frame can be expressed as a superposition of states $|p; JM; \lambda_1\lambda_2\rangle$ with definite total angular momentum (and vice versa).

In the process 1.17, since the electron rest energy m_e is negligible, the final state total helicity $\mu \equiv \lambda_{e^+} - \lambda_{e^-}$ can only be $\mu = \pm 1$. This is equivalent to saying that, at high energy, helicity is conserved in a QED vertex. The helicity λ of the $\bar{p}p$ system can be ± 1 or 0, $\lambda = 0$ being suppressed as the CM energy becomes much larger than the proton rest energy. The dominant process is the exchange of one virtual photon, and therefore the total angular momentum J of the initial and final state is 1. It follows that there are six amplitudes describing the process, whose squared moduli have to be summed for unpolarized scattering:

$$\begin{array}{lll} A_{+1,+1}\, d^1_{+1,+1} & A_{0,+1}\, d^1_{0,+1} & A_{-1,+1}\, d^1_{-1,+1} \\ A_{+1,-1}\, d^1_{+1,-1} & A_{0,-1}\, d^1_{0,-1} & A_{-1,-1}\, d^1_{-1,-1}. \end{array} \tag{1.21}$$

Parity conservation and charge conjugation symmetry ensure that all $A_{\pm 1,\pm 1}$ are equal. Moreover, the d matrices satisfy the relations:

$$\begin{array}{lllll} d^1_{+1,+1} & = & d^1_{-1,-1} & = & \left(\frac{1+\cos\theta}{2}\right) \\ d^1_{+1,-1} & = & d^1_{-1,+1} & = & \left(\frac{1-\cos\theta}{2}\right) \\ d^1_{0,+1} & = & d^1_{0,-1} & = & \left(-\frac{\sin\theta}{\sqrt{2}}\right) \end{array} \tag{1.22}$$

Therefore, the unpolarized differential cross section contains two terms, the second of which is suppressed as the CM energy increases:

$$\frac{d\sigma}{d\Omega} \propto |A_1|^2 \left(1 + \cos^2\theta^*\right) + |A_0|^2 \sin^2\theta^*. \tag{1.23}$$

The detailed lowest-order QED calculation has been carried out referring to the analog of the diagram depicted in Figure 1.1 and using Equation 1.8 to parameterize the proton-antiproton current (Zichichi et al. 1962). If one indicates with β_p the speed of the (anti)proton in the CM frame,

$$\beta_p \equiv \sqrt{1 - \frac{4m_p^2}{s}}, \tag{1.24}$$

the differential cross section can be written as:

$$\left(\frac{d\sigma}{d\Omega}\right)_{\bar{p}p\,\to\,e^+e^-} = \frac{\alpha^2}{4\beta_p s}\cdot\left[|G_M|^2\left(1+\cos^2\theta^*\right)+\frac{4m_p^2}{s}|G_E|^2\sin^2\theta^*\right] \tag{1.25}$$

where θ^* is the CM angle between the positron and the antiproton tracks. If the final state particles are detected in a manner that does not distinguish between electron and positron, there is no interference contribution from next-order processes.

At low q^2 in the spacelike region, the Sachs form factors are strictly related to the charge and magnetic moment distributions inside the proton (Section 1.2). Expression 1.25 for the cross section, together with Equation 1.23, emphasizes a relativistic interpretation of G_M and G_E — they are proportional to the helicity conserving and non-conserving amplitudes, respectively.

The cross section of the inverse process has the same angular dependence and differs only by a phase-space factor (principle of detailed balance). It is (Cabibbo and Gatto 1961):

$$\left(\frac{d\sigma}{d\Omega}\right)_{e^+e^-\,\to\,\bar{p}p} = \beta_p^2\cdot\left(\frac{d\sigma}{d\Omega}\right)_{\bar{p}p\,\to\,e^+e^-} \tag{1.26}$$

Form factors in the timelike region are not guaranteed to be real. If the beam or the target are polarized, an azimuthal dependence of the cross section arises, allowing to separate the real from the imaginary part. Otherwise, only their moduli can be measured.

1.5 Review of the Timelike Measurements

All the measurements of the timelike magnetic form factor of the proton are briefly described to emphasize the experimental techniques employed and their evolution. The results are summarized in Table 1.1 and in Figure 3.22.

From the following discussion, the context in which experiment E-835 operated and the relevance of its data will emerge.

The first timelike experiment was carried out at CERN in 1965, using a partially-separated antiproton beam from the Proton Synchrotron (Conversi et al. 1965). The beam momentum, corresponding to $s = 6.8$ GeV^2, was chosen in order to maximize the number of expected events, taking into account the energy dependence of the antiproton yield and of the cross section. The beam was identified by means of a gas Čerenkov counter, which allowed to reject the dominant pion component. The interactions took place inside a polyethylene target. The two-arm telescope made of plastic scintillators, spark chambers and lead absorbers, was used to select e^+e^- and $\mu^+\mu^-$ final states in the region around 90° in the CM reference frame. After producing about 10^{10} antiproton-proton interactions, no events were observed. Upper limits on the form factors and on the total cross section were published. Assuming $|G_E| = |G_M|$, as it is at threshold, they obtained $\sigma(\bar{p}p \to e^+e^-) < 1.44$ nb (90% CL).

Tab. 1.1: All existent measurements of the magnetic form factor of the proton.

s (GeV^2)	$\|G_M\| \times 10^2$	N	Lab	Machine	Experiment	Year
3.52	51±8	29	CERN	PS	ELPAR	1977
3.52	53^{+6}_{-8}	1830	CERN	LEAR	PS-170	1994
3.55	39±5	34	CERN	LEAR	PS-170	1994
3.57	34±4	40	CERN	LEAR	PS-170	1994
3.60	31±3	50	CERN	LEAR	PS-170	1994
3.61	46^{+15}_{-9}	5	CERN	PS	ELPAR	1977
3.69	36±5	16	Frascati	Adone	FENICE	1994
3.69	28.1±1.4	348	CERN	LEAR	PS-170	1994

continued on next page

continued from previous page

s (GeV^2)	$\lvert G_M \rvert \times 10^2$	N	Lab	Machine	Experiment	Year
3.76	25.5±1.3	375	CERN	LEAR	PS-170	1994
3.8	39±6	16	Orsay	DCI	DM-1	1979
3.83	24.9±1.0	284	CERN	LEAR	PS-170	1994
3.9	25±8	9	Orsay	DCI	DM-1	1979
3.94	24.6±1.1	210	CERN	LEAR	PS-170	1994
4.0	26±3	22	Orsay	DCI	DM-2	1983
4.00	24±3	18	Frascati	Adone	FENICE	1994
4.1	26±3	27	Orsay	DCI	DM-1	1979
4.18	23.7±0.9	496	CERN	LEAR	PS-170	1994
4.2	22±2	24	Orsay	DCI	DM-2	1983
4.4	27±4	25	Frascati	Adone	Castellano et al.	1973
4.4	19±2	20	Orsay	DCI	DM-2	1983
4.41	22±2	28	Frascati	Adone	FENICE	1994
4.6	21±4	11	Orsay	DCI	DM-1	1979
4.6	17±2	17	Orsay	DCI	DM-2	1983
4.8	19±2	19	Orsay	DCI	DM-2	1983
5.0	14±4	3	Orsay	DCI	DM-2	1983
5.1	<20	–	BNL	AGS	Hartill et al.	1969
5.69	$8.4^{+1.7}_{-1.3}$	7	Orsay	DCI	DM-2	1990
5.95	15±3	7	Frascati	Adone	FENICE	1994
6.6	<16	–	BNL	AGS	Hartill et al.	1969
6.8	<25	–	CERN	PS	Conversi et al.	1965
8.9	<5.2	–	CERN	ISR	R-704	1985
8.9	$3.3^{+0.6}_{-0.4}$	14	FNAL	AA	E-760	1993
9.6	21±3	14	DESY	DORIS	DASP	1975
12.4	$1.3^{+0.3}_{-0.2}$	11	FNAL	AA	E-760	1993
12.5	<4.2	–	CERN	ISR	R-704	1985
13.0	$1.3^{+0.5}_{-0.3}$	4	FNAL	AA	E-760	1993

In 1969, other upper limits were estabilished by an experiment at the Alternating Gradient Synchrotron operating at Brookhaven National Laboratory, for $s = 5.1$ GeV^2 and 6.6 GeV^2 (Hartill et al. 1969). The incident antiprotons were identified by measuring the time of flight of the beam particles. A long cylindrical flask contained the liquid hydrogen target. The tracking system was based upon hodoscopes and spark chambers. An effective suppression of the pion background was obtained by placing lead-lucite Čerenkov shower counters outside the tracking detectors. No events compatible with the electron-positron hypothesis were found.

The first positive result came in 1973, from head-on electron-positron annihilation at Adone, the storage ring in Frascati (Castellano et al. 1973). An integrated luminosity of about 0.2 pb^{-1} was collected at $s = 4.4$ GeV^2. Several criteria were used to identify the slow proton or antiproton tracks. Range and energy loss measurements were provided by a series of scintillation counters. Coplanarity and collinearity of the tracks were measured with a hodoscope and a spark chamber and contributed to suppress cosmic rays and beam-related background, like other two-body reactions or beam-gas scattering. Cosmic rays were also rejected by looking at the time of the event relative to a signal in phase with the accelerating RF cavity. From the twenty-five events observed, a cross section $\sigma(e^+e^- \to p\bar{p}) = (0.91 \pm 0.22)$ nb was deduced.

Soon after the discovery of the J/ψ, in 1975, a measurement was done at that energy (corresponding to $s = 9.6$ GeV^2) at the electron-positron storage ring DORIS (DESY) by the DASP collaboration (Braunschweig et al. 1975). The goal was to observe two-body hadronic decays of the then called '3.1 GeV resonance'. In particular, the $\pi^+\pi^-$, K^+K^- and $p\bar{p}$ final states were selected, using the magnetic Double Arm SPectrometer, based upon momentum, range, shower and time-of-flight information. Fourteen antiproton-proton events were observed. After normalizing to the $e^+e^- \to$

$\mu^+\mu^-$ cross section, the ratios

$$\frac{\sigma(e^+e^- \to p\bar{p})}{\sigma(e^+e^- \to \mu^+\mu^-)} = \begin{cases} 0.036 \pm 0.010 & \text{(a)} \\ 0.030 \pm 0.009 & \text{(b)} \\ 0.022 \pm 0.006 & \text{(c)} \end{cases} \tag{1.27}$$

were obtained, corresponding to different assumptions on the angular distribution, namely: (a) negligible electric contribution, implying $(1 + \cos^2\theta^*)$; (b) a flat distribution; or (c) $|G_M| = 0$, implying $(1 - \cos^2\theta^*)$. Rescaling the previous measurements and limits, a clear excess was found, indicating the relevant role of the resonance in the process; the corresponding value of $|G_M|$ can be compared with values at similar energies in Table 1.1.

The value of the form factor at threshold was measured indirectly in antiproton-proton annihilations at the CERN PS in 1977 (Bassompierre et al. 1976; Bassompierre et al. 1977). This measurement was of particular interest, because at $s = 3.52$ GeV^2 the electric and magnetic form factors are strictly equal; moreover, the measurement was not feasible at electron-positron colliders, because of the phase-space suppression of the cross section (Equation 1.26) and because of the impossibility to detect the proton and the antiproton at rest. The measurement proceeded in two steps. The first phase of the experiment succeeded in discriminating antiprotons annihilating at rest from annihilations in flight in the liquid hydrogen target, with a negligible background. The selection was based upon pulse height in the scintillators and tracking and shower characteristics in the spark chambers. By selecting e^+e^- (29 events), $\pi^+\pi^-$ and K^+K^- (240 events total) final states, the e^+e^- branching fraction at rest could be measured:

$$B_{e^+e^-} = \frac{\Gamma(\bar{p}p \to e^+e^-)}{\Gamma(\bar{p}p \to \text{total})} = (3.2 \pm 0.9) \times 10^{-7} \tag{1.28}$$

The second step consisted in evaluating the total cross section times the antiproton momentum at threshold. That was done by extrapolating existing data taken at low energy, obtaining $(\sigma_{tot} \times p_{lab})_{thr} = (56 \pm 2)$ mb × (GeV/c). From $B_{e^+e^-}$ and the product $(\sigma_{tot} \times p_{lab})_{thr}$, the magnetic form factor at threshold could be deduced. A measurement at $s = 3.61$ GeV^2 was also published by the same experiment, based upon five events. Both measurements rely on the $|G_E| = |G_M|$ hypothesis and on the assumption that e^+e^- and two-hadron events have the same angular distribution.

More data were collected in e^+e^- collisions at DCI (Orsay) starting from 1979 (Delcourt et al. 1979). The energy range scanned corresponds to s between 3.7 and 5.7 GeV^2. The DM1 detector consisted of four cylindrical multiwire proportional chambers inside a solenoid. Outside, a set of liquid scintillator counters was used to reject cosmic rays, which represented the main background. The head-on beam collisions took place in a 30 cm region and an integrated luminosity of 0.4 pb^{-1} was accumulated. A total of 63 $p\bar{p}$ events were observed, using the momentum information and the beam synchronization to identify them; also, the tracks were required to stop in the magnet yoke. The results were grouped in four points.

Three series of runs, corresponding to a total of about 0.7 pb^{-1}, were acquired with the DM2 detector in 1982 and 1984 (Bisello et al. 1983; Bisello et al. 1990). Inside a cylindrical solenoid two multiwire proportional chambers and several layers of drift chambers were placed. Still inside the magnet yoke were a segmented water Čerenkov counter and a series of scintillation counters, used for time-of-flight and energy deposit measurements. Collinear pairs were selected using momentum measurements. The shower detectors outside the solenoid, made of layers of lead, scintillator and streamer tubes, allowed to discriminate between e^+e^- and $\mu^+\mu^-$

pairs. These events served as a normalization for the 112 $p\bar{p}$ events, which were identified by range measurements and by detecting the antiproton annihilation products. Given the wide angular acceptance of the detector ($|\cos\theta^*| < 0.7$), it was possible to observe the angular distribution of the events. The best fit indicated a value of $|G_M| / |G_E| = 0.34$ for $s \leq 5$ GeV^2; but the low statistics still allowed the $|G_E| = |G_M|$ hypothesis to be highly compatible with the data.

The first high statistics data near threshold were collected at the CERN Low Energy Antiproton Ring by experiment PS-170 (Bardin et al. 1991a; Bardin et al. 1991b; Bardin et al. 1994). The number of events observed in that region was increased by more than an order of magnitude. For the first time, a relatively precise measurement of the angular distribution was also possible at different energies. The high-intensity ($\approx 2 \times 10^6$ particles/s) antiproton beam impinged on a liquid hydrogen target, placed in the gap of a C-shaped magnet. Momentum measurement was achieved using the tracking information provided by drift tubes. A ring of gas Čerenkov counters and shower detectors allowed to separate electron and positrons from pion and kaon pairs, which were used for cross-section normalization. Since the antiproton range in liquid hydrogen was well known, the reconstructed vertex position determined the momentum of the incoming antiproton, and annihilations were observed both at rest and in flight. The angular distribution of the events, measured up to $|\cos\theta^*| = 0.8$, was compatible with the $|G_E| = |G_M|$ hypothesis. This experiment revealed a much steeper slope of $|G_M|$ versus q^2 compared to what previous low-statistics experiments seemed to indicate.

Significant improvements in luminosity came from the exploitation of antiproton storage rings and hydrogen jet targets, used at CERN (Baglin

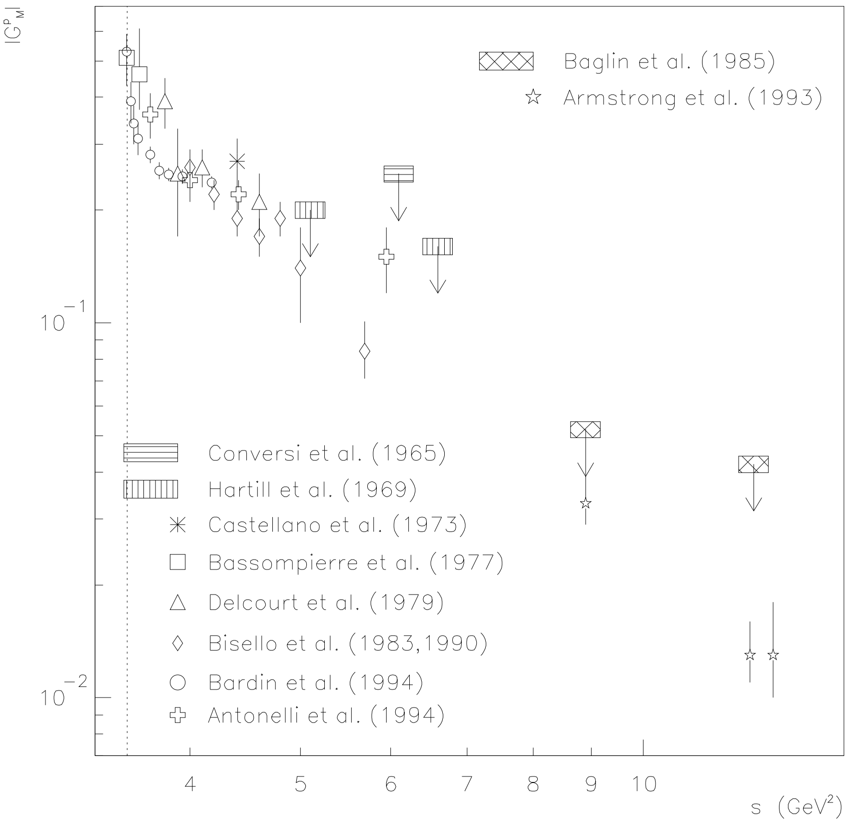

Fig. 1.3: Existing data on the magnetic form factor of the proton. Results corresponding to the $|G_E| = |G_M|$ hypothesis are reported. The cross-hatched rectangles represent upper limits at the 90% confidence level.

et al. 1985) and later at Fermilab (Armstrong et al. 1993). The antiproton storage rings provide stochastically cooled ($\Delta p/p$ better than 10^{-3}) and intense ($\approx 10^{10}$ particles) antiproton beams. The hydrogen jet targets can reach high densities without compromising the beam stability[b]. Cross sections in the picobarn range became accessible, and detectors able to extract such small signals were devised. The high-q^2 region, where quantitative predictions are more easily calculable, began to be open to experimental investigation.

Experiment R-704 at the CERN Intersecting Storage Ring reached instantaneous luminosities of 3×10^{30} cm^{-2} s^{-1} (Baglin et al. 1985). The main goal of the experiment was to study the electromagnetic decays of the charmonium resonances, produced in $\bar{p}p$ annihilations. The detector was therefore apt to identify e^+e^- final states. Each of the two arms of the non-magnetic spectrometer consisted of a tracking system, a gas Čerenkov counter to tag electrons and an electromagnetic calorimeter. An attempt to sample the high-q^2 behavior of the form factors was made, by selecting $s = 8.9$ GeV^2 and $s = 12.5$ GeV^2. No events were observed and upper limits were set.

Fermilab experiment E-760 had similar goals and used a similar technique, but could exploit better performing beam, target and detectors during its data taking in 1990 and 1991 (Armstrong et al. 1993). The beam stored in the Antiproton Accumulator ($\approx 10^{11}$ particles/store) intersected the hydrogen gas jet target, achieving instantaneous luminosities up to 9×10^{30} cm^{-2} s^{-1}. The interaction region was confined in less than a cubic centimeter. Several charmonium resonances in the range 8.9 GeV$^2 < s <$ 13.0 GeV^2 were scanned with a non-magnetic spectrometer designed to de-

[b] Because of their relevance for the results presented in this dissertation, the Fermilab Antiproton Source and the E-835 hydrogen jet target are described in more detail in Chapter 2.

tect electromagnetic final states, like e^+e^-X or $\gamma\gamma$. The cylindrical detector covered the full azimuthal region around the beam axis and the polar interval between approximately 15° and 65° in the laboratory frame. Its main parts were a tracking system (made of two hodoscopes, a straw chamber, a radial projection chamber, a multiwire chamber and two layers of streamer tubes), a threshold Čerenkov detector to identify electrons at the trigger level, and a lead-glass electromagnetic calorimeter. The electron (or positron) tagging was based upon pulse height in one of the hodoscopes, Čerenkov signal, energy deposition in the radial projection chamber and transverse shape of the shower in the calorimeter. A total of 29 background-free e^+e^- events were observed.

Experiment E-835 at Fermilab, whose data and results are the object of this dissertation, used the upgraded E-760 apparatus (Armstrong et al. 1992b). Some important modifications were made for the data-taking run, which lasted from October 1996 through September 1997 and allowed to collect a total of 143 pb^{-1}. The experiment is described in detail in Chapter 2.

Before its final shutdown in 1993, and about twenty years after allowing the first measurement of the timelike form factor to be made, the Adone ring was used by the FENICE experiment to measure the neutron form factor for the first time. The detector was also suitable for observing $p\bar{p}$ final states (Antonelli et al. 1994). It consisted of a central detector and of an antinucleon detector, arranged in an octagonal geometry around the beam pipe. In the central detector were a layer of scintillators for triggering and for time-of-flight measurements, and four planes of streamer tubes, used for tracking. The antinucleon detector was designed to recognize annihilation stars. It was made of iron plates, scintillator slabs and streamer tube planes. Four energy regions were explored, with a total luminosity of about $0.3\ \text{pb}^{-1}$.

1.6 Form Factors in Quantum Chromodynamics. Attempts to Explain the Proton Structure

At present, Quantum Chromodynamics cannot predict the form factors of hadrons. Several approximations and models that are calculable have been devised, all with a limited range of applicability. The difficulties arise from the fact that in the understanding of elastic hadronic processes, both a small and a large distance picture contribute. In other words, asymptotic freedom and the perturbative approach play an important role at high momentum transfer; at the same time, the hadron conserves its identity, so the confinement of quarks and gluons must be taken into account as well. For these reasons, it is considered an interesting and challenging field of theoretical research.

Here, I briefly discuss the approach of valence perturbative QCD. Detailed information and references can be found in the review article by Sterman and Stoler (1997).

Valence perturbative QCD is applicable at high momentum transfer, even though there is no agreement upon how high q^2 has to be. In this regime, the quark masses can be neglected and a first-order perturbative approach in terms of $\alpha_s(q^2)$ is possible. Also, the dominant contributions come from hadronic states with the lowest number of partons (*valence* partons), i. e. $q\bar{q}$ for mesons and qqq for barions. In this framework, the pion form factor[c] can be calculated (Lepage and Brodsky 1980):

$$F_\pi(Q^2) = 16\pi f_\pi^2 \frac{\alpha_s(Q^2)}{Q^2}, \tag{1.29}$$

where $f_\pi \simeq 93$ MeV is a dimensional constant that can be experimentally extracted from the analysis of pion decays. Unfortunately, the existing data on the charged pion form factor is at relatively low Q^2 and it is affected by systematic uncertainties. On the other hand, π^0 data is in good agreement with Equation 1.29 already at $Q^2 \simeq 6$ (GeV/c)^2.

The asymptotic functional form of the proton magnetic form factor versus Q^2 is known up to an overall constant C (Lepage and Brodsky 1980):

$$G_M(Q^2) = \frac{32\pi^2}{9} C^2 \frac{\alpha_s^2(Q^2)}{Q^4} \left(\ln \frac{Q^2}{\Lambda^2}\right)^{-4/27}, \tag{1.30}$$

where Λ is the QCD scale parameter. The running coupling constant, to the leading logarithmic term, can be written as:

$$\alpha_s(Q^2) \simeq \frac{4\pi}{9} \left(\ln \frac{Q^2}{\Lambda^2}\right)^{-1}. \tag{1.31}$$

Asymptotically, the form factors in the timelike region are equal to those in the spacelike region (Gousset and Pire 1995). At lower energies, timelike form factors are approximately twice as large as the spacelike ones, as demonstrated by Gousset and Pire (1995) in the case of mesons; Kroll et al. (1993) showed that barion form factors behave similarly, but only within the additional approximations of the quark-diquark model.

As anticipated in Section 1.3, there is good agreement between these semi-quantitative predictions and the data. Obviously, more experimental information and theoretical speculations are necessary in order to fully understand the electromagnetic properties of the proton.

[c] Having the pion spin zero, only one form factor is necessary to characterize its electromagnetic properties.